Available online at www.sciencedirect.com

ScienceDirect

Acta Materialia 71 (2014) 176–184

Acta MATERIALIA

www.elsevier.com/locate/actamat

Adaptive ferroelectric state at morphotropic phase boundary: Coexisting tetragonal and rhombohedral phases

Yang Zhang [a], Dezhen Xue [a,*], Haijun Wu [a,b,*], Xiangdong Ding [a], Turab Lookman [c], Xiaobing Ren [a,d]

[a] Multi-disciplinary Materials Research Center, Frontier Institute of Science and Technology, State Key Laboratory for Mechanical Behavior of Materials, Xi'an Jiaotong University, Xi'an 710049, China

[b] Department of Physics, South University of Science and Technology of China, Shenzhen 518055, China

[c] Theoretical Division and Center for Nonlinear Studies, Los Alamos National Laboratory, Los Alamos, NM 87545, USA

[d] Ferroic Physics Group, National Institute for Materials Science, Tsukuba, 305-0047 Ibaraki, Japan

Received 4 October 2013; received in revised form 3 March 2014; accepted 3 March 2014

Abstract

With a focus on local symmetry, the microstructural basis for high piezoelectric performance in $PbMg_{1/3}Nb_{2/3}O_3$–$xPbTiO_3$ (PMN–PT) ceramics at the morphotropic phase boundary (MPB) composition was investigated by means of convergent-beam electron diffraction analysis and twin diffraction pattern analysis. The local structure was found to consist of coexisting (1 0 1)-type tetragonal nanotwins and (0 0 1)-type rhombohedral nanotwins. A phenomenological theory based on crystallography is proposed to show that such nanoscale coexistence can give rise to an average monoclinic structure through strain accommodation. The average monoclinic structures (Ma and Mc) vary with temperature and composition due to the dependence on temperature and composition of the lattice parameters. Based on in situ X-ray diffraction data, we demonstrate how the polarization rotates across the MPB region in PMN–PT ceramics with varying temperatures and compositions.

Keywords: Piezoelectrics; Morphotropic phase boundary; TEM; Twin boundary; Adaptive phase

1. Introduction

The most useful piezoelectric materials, such as $PbZr_{1-x}Ti_xO_3$ (PZT) [1–3], $PbMg_{1/3}Nb_{2/3}O_3$–$xPbTiO_3$ (PMN–PT) [4–7] and $PbZn_{1/3}Nb_{2/3}O_3$–$xPbTiO_3$ (PZN–PT) [8], display a transition region, referred to as the morphotropic phase boundary (MPB), in their composition–temperature phase diagrams. This has served as the basis for understanding the remarkable electromechanical response in applications [9–11]. In general, the MPB separates the phase of tetragonal (T) symmetry from rhombohedral (R) symmetry [12,13]. It therefore raises the question: how is it possible to smoothly transform from one phase to the other when there is no group–subgroup relationship between T and R? [14]. Probing the microstructure of such a transition from symmetry R to T can be considered to be an effective way to understand the non-group–subgroup transition [15].

We know from symmetry that a non-group–subgroup transition can be mediated by a common subgroup of both T and R [13,14]. Neutron diffraction and X-ray diffraction (XRD) investigations on PMN–PT, PZN–PT and PZT

* Corresponding authors. Address: Multi-disciplinary Materials Research Center, Frontier Institute of Science and Technology, State Key Laboratory for Mechanical Behavior of Materials, Xi'an Jiaotong University, Xi'an 710049, China (H. Wu).

E-mail addresses: xuedezhen@mail.xjtu.edu.cn (D. Xue), wu.hj@sustc.edu.cn (H. Wu).

http://dx.doi.org/10.1016/j.actamat.2014.03.007

1359-6454/

single crystals and ceramics have shown the presence of a monoclinic (M) phase linking T and R in the MPB region [16,17]. The single M phase is considered a reasonable intermediate phase because the M symmetry (Cm or Pm) is the subgroup of both T symmetry (P4mm) and R symmetry (R3m) [13]. A key feature of this structure is that the polarization vector is no longer constrained to lie along a symmetry axis, as in the R and T structures, but instead can rotate within the monoclinic plane [18]. However, the heterogeneous microstructure in the vicinity of the MPB has been investigated over the last 20 years [19,20] and a number of recent studies have shown that such nanoscaled heterogeneity consists of either R or T symmetry rather than M symmetry [15,21–23]. The evidence for a single M phase, i.e. the appearance of M intensities in diffraction patterns, can also be considered a result of coherence effects amongst the nanoscaled structures [19–24]. The MPB region is thus regarded as inhomogeneous at the nanoscale (with R or T symmetry) but homogeneous at larger scales (with M symmetry) [19,20,23–26].

An adaptive state, formed via strain accomodation, has been proposed to show that the average M symmetry found for the MPB could be considered a result of coherence effects of R (or T) nanodomains [21,25–29]. Three types of adaptive states with M symmetry are known, namely, Ma, Mb and Mc [30]. The former two Ma, Mb (Cm) states are obtained by shearing primitive unit cells along the pseudo-cubic $(1\,1\,0)_{pc}$ plane, the polarization $[uuv]$ of which is confined to the pseudo-cubic $(1\,-1\,0)_{pc}$ plane with $u > v$ and $u < v$, respectively, as schematically shown in Fig. 1a [30,31]. The other Mc (Pm) phase results from shearing primitive unit cells along the pseudo-cubic $(1\,0\,0)_{pc}$ plane. The polarization along $[u0v]$ is thus constrained to lie within the $(0\,1\,0)_{pc}$ plane, as shown in the schematic in Fig. 1a [30,31]. Transmission electron microscopy (TEM) experiments and lattice parameter analysis based on XRD in PMN–PT and PZN–PT have identified that the average symmetries of (0 0 1)-type R nanotwins [27,29], (1 1 0)-type R nanotwins [27,29] and (1 0 1)-type T nanotwins [21,24–26,32,33] are Ma, Mb and Mc symmetries, respectively.

The average structure can be any, or some combination, of the states Ma, Mb and Mc depending on temperature [34–36], composition [37,38], electric [8,36,39] and stress [31,36,40] fields. However, the local structure has so far been shown to be either nanoscaled R or T twins in the vicinity of the MPB in PMN–PT, PZN–PT and PZT piezoelectric materials [15,21,22,24]. Thus, it is still unclear how the M adaptive states (Ma, Mb or Mc) with distinct local structures transform from one structure to the other. This is especially the case for transformations between Ma and Mb with local R symmetry and Mc with local T symmetry.

A number of studies have indicated that local R and T structures can coexist within the microstructure. For example, the thermodynamics of coexistence of T and R heterophase polydomains at the MPB in ferroelectric films has been considered within the theory of elastic domains [41,42]. The volume fractions of the phases and different twin components have been obtained as functions of misfit strain and film orientation by applying an external field [41,42]. Recent high resolution XRD and TEM observations on epitaxial $BiFeO_3$ films have shown that R and T twins can coexist in the MPB region of $BiFeO_3$ [43,44]. In the case of very low domain wall energy and fine domains, the average symmetry of $BiFeO_3$ is monoclinic [31,45]. The large electromechanical response may be understood on the basis of electric field or strain-driven inter-conversion between R and T coexisting phases near the MPB [43,44]. These results imply that the microscopic origin of high electromechanical response in PZT, PMN–PT and PZN–PT near the MPB may be attributed to phase

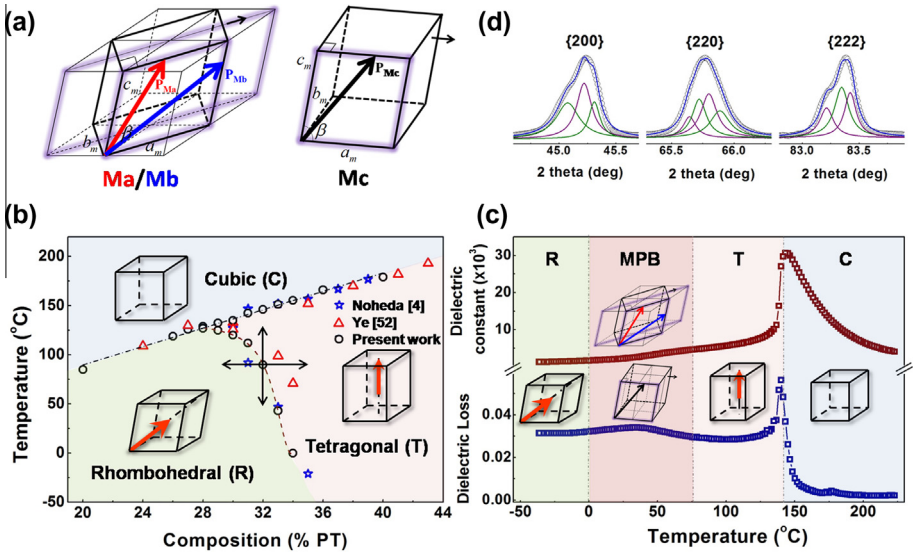

Fig. 1. (a and b) Phase diagram of PMN–xPT near the MPB composition. (c and d) Dielectric permittivity (ε) vs. temperature (T) curves for PMN–32PT. Three kinds of adaptive states with M symmetry, namely, Ma, Mb and Mc, can be found around the MPB region.

coexistence of nanoscale R and T regions [46–49]. Furthermore, the presence of two different local symmetries that can give rise to one average structure also occurs in ferroelastic/martensite systems [50].

In this study we performed TEM observation on PMN–PT ceramics at the MPB composition. We find local coexistence and ordering of T and R nanotwins at the MPB from detailed convergent-beam electron diffraction (CBED) analysis and twin diffraction pattern analysis. Based on our experimental observations, we propose a phenomenological model in which the M average symmetry can be viewed as a result of strain accomodation involving coherent matching of both the nanoscaled R twins and T twins. The monoclinic structure, as a function of the volume fraction of R (or T) nanodomains, hence represents a bridge between the R and T phases. The lattice parameters of R and T phases vary with temperature and composition, thereby influencing the volume fraction of R (or T) nanodomains. We also demonstrate how the polarization vector rotates across the MPB region in PMN–PT ceramics on varying the temperature and composition.

2. Experimental procedures

PMN–xPT ceramics with $20 \leqslant x \leqslant 40$ were synthesized by a modified "columbite-type" route using PbO (>99%), MgO (>99.5%), Nb_2O_5 (>99.95%) and TiO_2 (>99.9%) powders [51]. The sintered samples were polished to obtain the parallel sides and painted with silver electrodes for dielectric measurements. Average structural information was collected by in situ XRD measurements with a temperature accuracy of ±5 °C. The samples for the XRD measurements were annealed at 250 °C for 8 h to release possible internal stresses due to polishing. TEM sample preparation was performed by subsequent cutting, polishing, dimpling and ion milling. High-resolution electron microscopy and convergent-beam electron diffraction (CBED) were carried out using a JEM-2100F microscope.

3. Experimental results

3.1. Transition behavior of PMN–32PT ceramics

The phase diagram of the PMN–xPT system is shown in Fig. 1b. It was determined by measuring dielectric permittivity (ε) vs. temperature (T) curves and is consistent with that found by Noheda et al. [4] and Ye et al. [52], and these are also plotted in Fig. 1b. The MPB is located in the transition region between R and T phases, where the average structure Ma/Mb/Mc can be found. We chose the MPB composition PMN–32PT ceramic for our TEM observations. The temperature dependence of the dielectric permittivity and dielectric loss for PMN–32PT shown in Fig. 1c reveals a broadening dielectric anomaly between 0 °C and 75 °C. Such an anomaly indicates a sluggish phase transition over a wide temperature range, conventionally linked to MPB phenomena [4,52]. At a room temperature of 20 °C and in the MPB state, the XRD peak profiles are consistent with a superposition of T and R profiles, as shown in Fig. 1d. Thus, the microstructure of MPB can be obtained at room temperature and the ferroelectric–ferroelectric transition across the MPB can be achieved by two approaches: by varying the composition (along the horizontal line in Fig. 1b), as well as by varying the temperature (along the vertical line in Fig. 1b).

3.2. Convergent-beam electron diffraction analysis

The bright field (BF) TEM image in Fig. 2a shows two types of miniaturized nanodomains along [0 0 1] and [1 0 1] directions with a width of 10–50 nm in PMN–32PT. This was taken at room temperature (20 °C) with the electron-beam incident in the direction of pseudo-cubic [0 1 0]. In order to further verify the local coexisting crystal symmetry in the MPB region, we employed the CBED technique. The CBED method, with a probe size of a few nanometers (0.5–2.4 nm), can detect symmetry information within each nanodomain [15,53–57]. The two sides of the MPB show R and T symmetry, with a space group of R3m and P4mm, respectively. It is easy to differentiate them in the CBED pattern along the [0 1 0] zone axis: the R structure has a (1 0 −1) or (1 0 1) mirror plane, whereas the T structure has a (1 0 0) or (0 0 1) mirror plane. Fig. 2b1 and 2b2, taken from the adjacent nanodomains (marked R in Fig. 2a), show (1 0 −1) and (1 0 1) mirror planes, respectively, indicating a local R symmetry. With the nanodomain wall direction along [0 0 1], the polarization direction in each nanodomain can be identified along [1 1 1] and [−1 −1 1], which is a typical (0 0 1) type 109° R nanotwin. In contrast, Fig. 2c1 and c2, taken from adjacent nanodomains (marked as T in Fig. 2a), show (1 0 0) and (0 0 1) mirror planes, respectively, indicating a local T symmetry. The polarization direction in each nanodomain must be along [0 0 1] and [1 0 0], which is typical of (1 0 1) type 90° T nanotwins [58]. Thus, our results show that the microstructure at the MPB in PMN–32PT is composed of (1 0 1)-type tetragonal (T) nanotwins and (0 0 1)-type rhombohedral (R) nanotwins.

3.3. Twin diffraction pattern analysis

Fig. 3 provides additional evidence of the nanoscale coexistence of R and T twins from twin diffraction pattern analysis. Two types of nanodomains along [1 0 1] and [0 0 1] for the [0 1 0] zone axis can be found in Fig. 3a. Fig. 3b1 and b2 show the simulated twin diffraction pattern for the (0 0 1)-type R twin and (1 0 1)-type T twin for [0 1 0] zone axis, including two key structural features: the un-split row of reflection spots (USR) and the split spots (Δg). The former (USR), contributed by two twin variants with coincident lattices in reciprocal space, corresponds to the twin plane shared between two twin variants in real space. The Δg (the difference of g vectors $\Delta g = g_1 - g_2$) is caused by a slight discrepancy in simultaneously reflecting g vectors

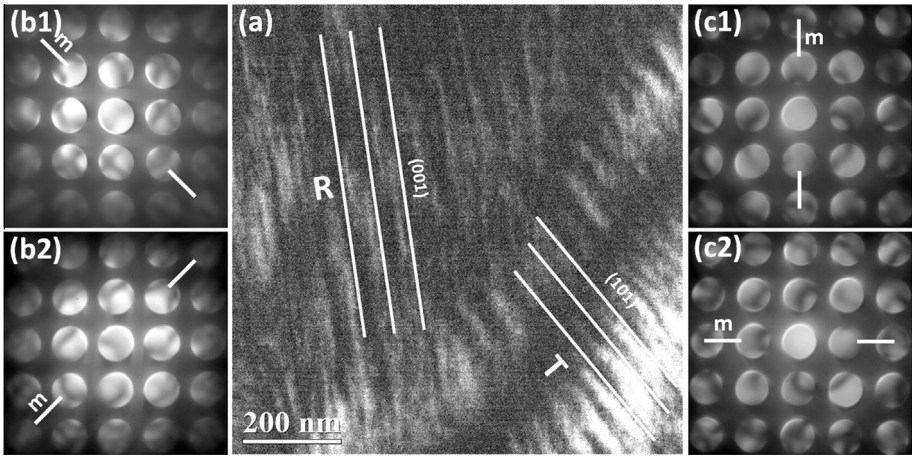

Fig. 2. (a) Bright-field (BF) image of MPB domains on [0 1 0] zone axis. In order to probe the nanodomains clearly, the morphology was imaged several degrees off the [0 1 0] zone axis. (b1 and b2) The CBED patterns obtained from two adjacent nanodomains along [0 0 1]. (c1 and c2) The CBED patterns obtained from two adjacent nanodomains along [1 0 1].

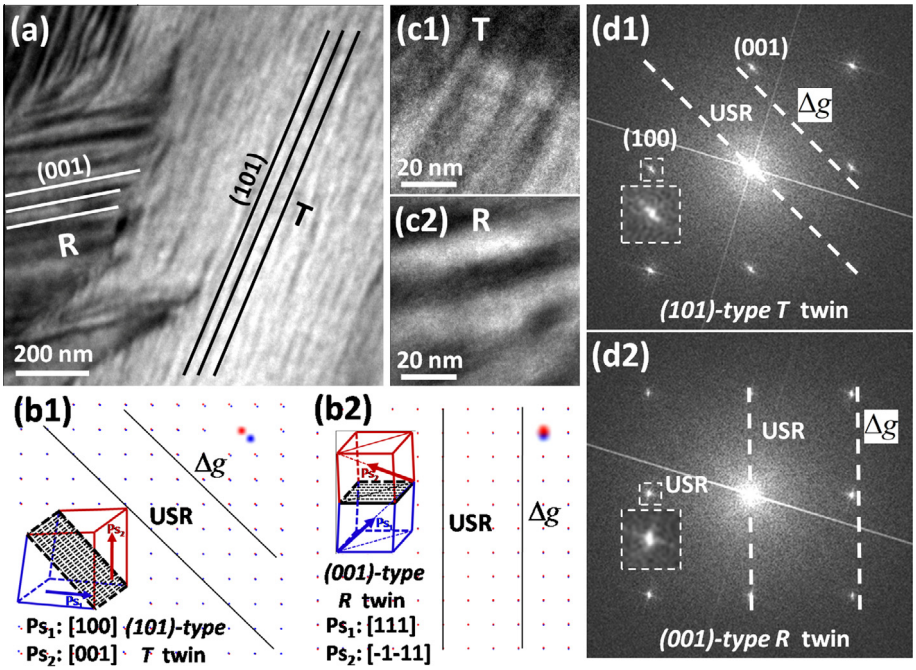

Fig. 3. (a) BF image of MPB domains on [0 1 0] zone axis. In order to probe the nanodomains clearly, the morphology was imaged several degrees off the [0 1 0] zone axis. (b1 and b2) simulated twin diffraction pattern for (1 0 1)-type T twin and (0 0 1)-type R twin on [0 1 0] zone axis. The symbols "Δ*g*" and "USR" stand for spot split and unsplit row of reflection spots in the twin diffraction pattern. (c1 and c2) HREM images of nanodomains along [1 0 1] and [0 0 1]. (d1 and d2) Fourier-filtered transformation (FFT) images of (c1) and (c2). The FFT images are slightly tilted for clarity.

from two individual crystal variants [51,59]. For the [0 1 0] zone axis, the unique situation of *USR*//Δg for (1 0 1)-type T twin is along [1 0 −1] and that for (0 0 1)-type R twin is along [0 0 1], as shown in Fig. 3b1 and b2. One can thus utilize such twin diffraction analysis to distinguish R and T twins. However, the difference in lattice constants between R and T in PMN–PT is too small to be identified in selected area electron diffraction patterns, especially for the nano-scaled domains. We thus chose to perform fast Fourier transforms (FFTs) on high-resolution electron microscopy (HREM) images to differentiate the R nanotwins from T nanotwins. HREM images of [1 0 1]-type and [0 0 1]-type nanodomains in Fig. 3a are shown in Fig. 3c1 and c2 and their corresponding FFT images are shown in Fig. 3d1 and d2. The enlarged 100 reflection spot shown in the inset of Fig. 3d1 undergoes an obvious change in Δ*g* along [1 0 −1], which is parallel with USR, indicating a (1 0 1)-type T twin. The (1 0 0) reflection spot in Fig. 3d2 satisfies the situation USR//Δ*g* along the [0 0 1] direction, indicating a (0 0 1)-type R twin. Thus, combining the CBED analysis, the local structure of MPB can be inferred to consist of a coexistence of nanotwinned R and T phases.

We note that at the MPB composition the average structure has been known to be monoclinic and consists of nanoscaled inhomogeneous microstructures. However, the average monolcinic structure was obtained by considering either local R nanotwins or local T nanotwins, but not both. We have observed a mixture of R nanotwins and T nanotwins in the MPB region. We thus propose a phenomenological model of the adaptive, strain accommodated state by considering coexisting local phases of R and T nanotwins and show how they lead to the average structure (monoclinic).

4. Model

4.1. Adaptive phase model for coexisting R and T twins

We consider a strain-accommodated phase, which is a coherent mixture of nanoscale R and T twins. Such an adaptive phase can be achieved by adjusting the volume fraction of each phase and the thickness of each variant within the phase to establish macroscopic strain invariance at the habit plane. Doing so eliminates long range stress fields generated by crystal lattice misfits. The condition for a stress-free adaptive state requires the transformation strain averaged over several variants to be an invariant plane strain (IPS), where the invariant plane is parallel to the habit plane [25,60].

During transformation, the pure distortions of the two product-phase twin variants with respect to the parent-phase lattice can be described by two deformation gradient matrixes F_1 and F_2. For convenience, we set the principal axes of F_1 to coincide with that of the untransformed parent phase. Then the relative rotation matrix Φ is given by the product of the coordinate transformation matrix, A, required to align the principal axes of F_2 with F_1, and the rotation matrix B which uses the twin plane normal of each twin variant before rotation, i.e.

$$\Phi = A^{-1} \cdot B \cdot A \tag{1}$$

where $A = \begin{pmatrix} \cos\beta & \cos\delta\cos\gamma & \cos\delta \\ -\cos\delta & \cos\beta\cos\gamma & \cos\beta \\ 0 & -\cos^2\delta - \cos^2\beta & \cos\gamma \end{pmatrix}$ is the coordinate transformation matrix, which changes the rotation axis to one of the principal axes (z axis here) and $[\cos\delta, \cos\beta, \cos\gamma]$ is the rotation axis. The matrix $B = \begin{pmatrix} \cos\theta & -\sin\theta & 0 \\ \sin\theta & \cos\theta & 0 \\ 0 & 0 & 1 \end{pmatrix}$ is the rotation matrix about the principal z axis and θ is the rotation angle.

The total distortion F can be then written as

$$F = xF_1 + (\mathbf{1} - x)\Phi \cdot F_2 \tag{2}$$

where x is the volume fraction of one orientational variant of the product-phase twin crystal. The deformation, F, is then a function of the volume ratio x and the lattice parameters of the parent and product phases [25].

In order to provide a stress-free boundary between the product-phase twins and parent-phase matrix along the IPS plane, the necessary and sufficient condition is that one of the principal distortions be unity, i.e. one of the principle strains vanishes. From WLR theory [61,62], such a condition can be satisfied by

$$\det(F \cdot F^* - I) = \mathbf{0} \tag{3}$$

where F^* is the transpose of F and I is a unit matrix and det is the determinant of the square matrix $F{\cdot}F^* - I$. Combining Eqs. (1)–(3), we can obtain a polynomial equation in terms of x, and obtain a suitable solution for x after neglecting the higher order terms with small coefficients.

In the present case there are (0 0 1)-type R twins with two variants along [1 1 1]/[−1 −1 1] R axis and (1 0 1)-type T twins with two variants along [1 0 0]/[0 0 1] T axis, as shown in Fig. 4a1 and a2 and 4b1 and b2. The total distortion matrices for (0 0 1) R and (1 0 1) T twins can be described by $R = \mu R_1 + (1-\mu)\Phi_R{\cdot}R_2$ and $T = \upsilon T_1 + (1-\upsilon)\Phi_T{\cdot}T_2$, respectively. The volume fractions μ and υ are for the [1 1 1] variants of R twins and [1 0 0] variants of T twins, respectively. For PMN–32PT (MPB composition at room temperature), the lattice parameters are $(\alpha, a_r) = (89.91566°, 0.4012426\ \text{nm})$, $(a_t, c_t) = (0.4001348\ \text{nm}, 0.4036841)$ and $a_c = 0.4012414$ nm. By applying the zero distortion condition to the IPS plane (Eq. (3)), we obtain the volume fractions $\mu_0 = 0.522304$, and $\upsilon_0 = 0.687248$.

We now consider the coexistence of two types of nanotwins, the (0 0 1)-type R twins and the (1 0 1)-T twins, as shown in Figs. 2 and 3. Fig. 4c and d provide a schematic illustration if we look along the [0 1 0] zone axis. Fig. 4c shows how the two types of twin lattices are adjoined with a coherent interface along $(1\,0\,1)_{pc}$. One T variant cannot match with two R variants along the (1 0 1) plane simultaneously, thus the interface is not strictly a plane, but a layer. Accordingly, in order to minimize the total energy, there must exist other distortions in the R–T interfaces, not present in pure R or T twin planes. This distortions can lead to curvature and blurring the interface [53], as shown in Figs. 2 and 3. Fig. 4d shows the coexistence of R twins, T twins and R–T coherent interfaces. The R–T interface is parallel to the T twin plane along $(1\,0\,1)_{pc}$, whereas the R twin plane is along $(0\,0\,1)_{pc}$. Accordingly, in Figs. 2 and 3, the projection traces of the nanodomain walls are directed along approximately [1 0 1] and [0 0 1], and these two types of nanodomains intersect along the [1 0 1] direction. In order to make R nanotwins coincident with T nanotwins along $(1\,0\,1)_{pc}$, Ψ_R and Ψ_T are used to describe the rotations of the principal axes of R nanotwins and T nanotwins relative to the axis of untransformed parent cubic phase. Since the distortion of R ($\theta_R = 0.12646°$) is quite small compared to that of T ($\theta_T = 0.505983°$) in PMN–PT (θ_R and θ_T are the rotation angles of R twin and T twin variants, respectively), Ψ_R can be neglected here. The matrix Ψ_T describes rotations along the [1 0 0] axis. That is, $\Psi_T = \begin{bmatrix} \cos\varphi & 0 & -\sin\varphi \\ 0 & 1 & 0 \\ \sin\varphi & 0 & \cos\varphi \end{bmatrix}$,

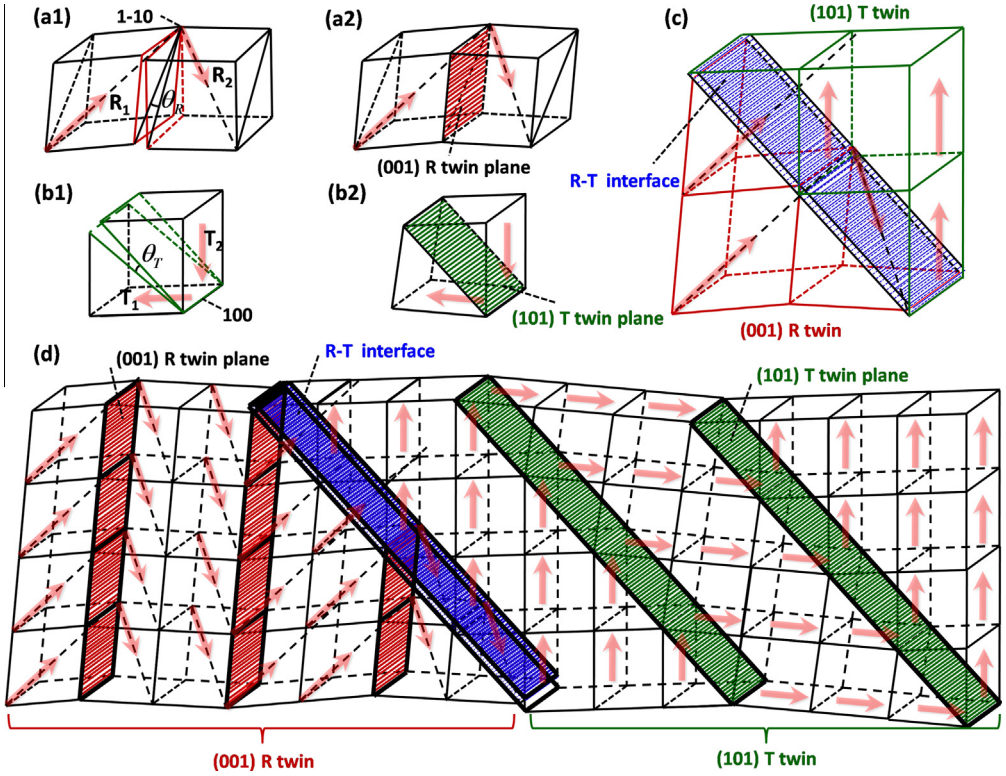

Fig. 4. Crystallographic illustrations of (0 0 1) R twin, (1 0 1) T twin and the coexistence of R and T twins. (a1 and a2) (0 0 1) R twin before and after rigid-body rotation, where the rotation axis [1 −1 0] and rotation angle θ_R are marked. The distortion or polarization vector in each variant is along [1 1 1] and [−1 −1 1], respectively, to form a head-to-tail pattern. (b1 and b2) (1 0 1) T twin before and after rigid-body rotation, where the rotation axis [0 1 0] and rotation angle θ_T are marked. The distortion or polarization vector in each variant is along [1 0 0] and [0 0 1], respectively, to form a head-to-tail pattern. (c) The coexistence of (0 0 1) R twin and (1 0 1) T twin, where the shearing planes marked with blue lines are along [1 0 1]. (d) Full picture of the coexistence of (0 0 1) R and (1 0 1) T twins. (For interpretation of the references to color in this figure legend, the reader is referred to the web version of this article.)

where $\varphi = \theta_T - \left(45^\circ - \arctan\frac{a_t}{c_t}\right)$. Thus, the total distortion matrix for the coexistence of (0 0 1) R twin and (1 0 1) T twins can be written as

$$E = \omega\Psi_R \cdot R + (\mathbf{1} - \omega)\Psi_T \cdot T \approx \omega R + (\mathbf{1} - \omega)\Psi_T \cdot T \qquad (4)$$

where ω and $1 - \omega$ are volume fractions of R nanotwins and T nanotwins, respectively. By applying the zero distortion condition to the IPS plane (Eq. (3)), we can obtain the values of volume fractions: $\omega_0 = 0.676829$. Thus the microstructure of PMN–32PT at 20 °C is composed of 2/3 R nanotwins and 1/3 T nanotwins approximately.

For ferroelectrics, each variant has a spontaneous polarization, with the same geometrical arrangement as the strain distortion in each variant. The average polarization of (0 0 1)-type R nanotwins is $\vec{P}_{AR} = \mu\vec{P}_{111} + (\mathbf{1} - \mu)\mathbf{\Phi}_R \cdot \vec{P}_{-1-11}$ and that of (1 0 1)-type T nanotwins is $\vec{P}_{AT} = \upsilon\vec{P}_{100} + (\mathbf{1} - \upsilon)\mathbf{\Phi}_T \cdot \vec{P}_{001}$, where $\vec{P}_{111}/\vec{P}_{-1-11}$ and $\vec{P}_{100}/\vec{P}_{001}$ are spontaneous polarizations along [1 1 1]/[−1 −1 1] of R twins and along [1 0 0]/[0 0 1] of T twins in the cubic axes. For the coexistence of these two types of nanotwins, the average polarization in general can be written as:

$$\vec{P}_A = \omega\vec{P}_{AR} + (\mathbf{1} - \omega)\mathbf{\Psi}_T \cdot \vec{P}_{AT} \qquad (5)$$

By substituting μ_0, υ_0 and ω_0 for the given composition (PMN–32PT) at room temperature 20 °C and $P_R = 0.33$ - C m^{-2}, $P_T = 0.37$ C m^{-2} (measured from the R composition PMN–29PT and T composition PMN–35PT) into Eq. (5), we get: $\underline{P}_{A0} = [0.0922659, 0.260719, 0.00997815]$. The polarization P_{A0} is the special adaptive polarization of the coexisting R nanotwins and T nanotwins, which corresponds to the condition of complete stress accommodation. We can see that P_{A0} corresponds roughly to Mc (polarization along [uv0], $u \neq v$), which is the widely reported average structure at MPB, especially in unpoled ceramics [4,25,26,38].

4.2. Polarization rotation with temperature and composition

We note that the volume fractions μ_0, υ_0 and ω_0 are dependent only on the crystal lattice parameters of the parent cubic phase and product R or T phases. The lattice parameters are functions of composition and temperature [25]. Thus, by changing temperature or composition, the rotation of the total adaptive polarization may be captured.

The lattice parameters of R and T can be calculated from in situ XRD measurements by fitting the profiles with R and T symmetry. The lattice parameters vs. temperature curves are shown in Fig. 5a. According to our model, the

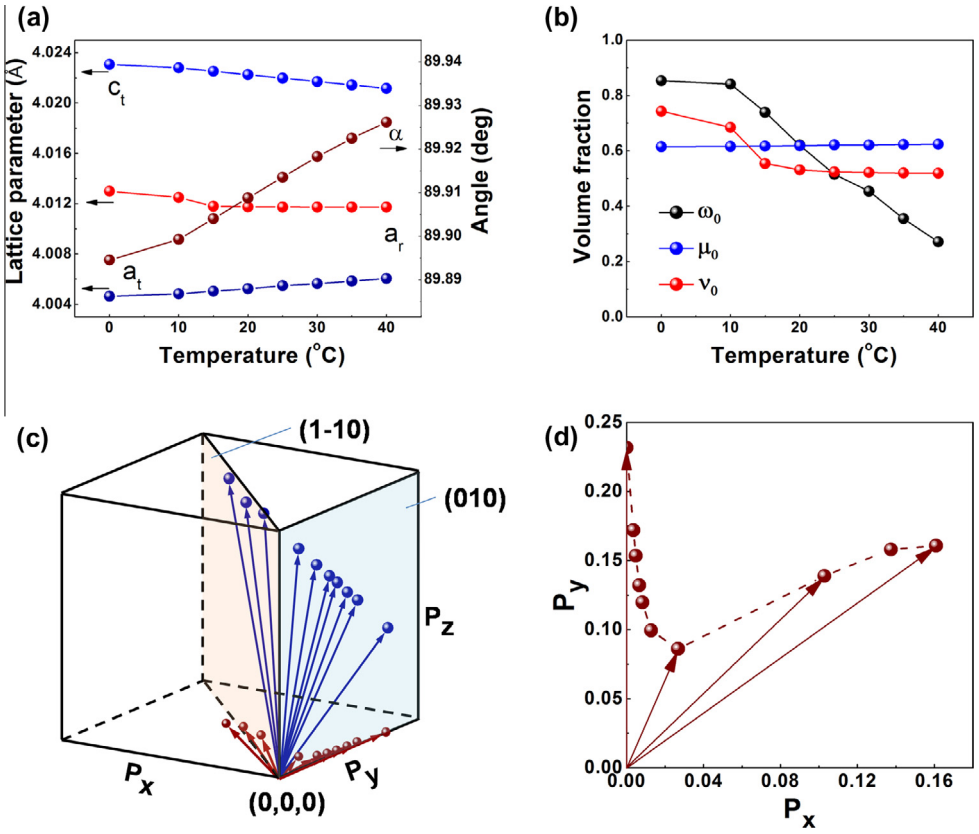

Fig. 5. (a) The lattice parameters vs. temperature curves. The lattice parameters of R and T can be calculated from in situ XRD measurements by fitting the profiles with R and T symmetry using the Lorentz function. (b) The volume fractions μ_0, υ_0 and ω_0 as a function of temperature. (c) The adaptive polarization vector in the MPB region as a function of temperature. (d) The X–Y projection of the adaptive polarization vector.

volume fractions μ_0, υ_0 and ω_0 as a function of temperature are shown in Fig. 5b. We find that the volume fraction of T nanotwins increases at the expense of R twins on heating from R-side MPB to T-side MPB. Fig. 5c shows that the adaptive polarization vector in the MPB region rotates gradually from a vector in the (001) plane (corresponding to Ma) to a vector in the (110) plane (corresponding to Mc) with increasing temperature [8,39]. The X–Y projection of the adaptive polarization vector in Fig. 5d shows the rotation process more clearly. Changing composition is similar to changing temperature. The lattice parameters and volume fractions μ_0, υ_0 and ω_0 as a function of composition are shown in Fig. 6a and b, respectively. The volume fraction of T nanotwins will increase at the expense of the R twin from the R-side MPB to the T-side MPB. The rotation of the adaptive polarization vector in the MPB region between $\langle 111\rangle_R$ and $\langle 100\rangle_T$ as a function of composition is shown in Fig. 6c and d [8,39].

We also found that most of the MPB region consists of the Mc ($P_{A0} \approx [uv\mathbf{0}], u \neq v$) phase, whereas the Ma ($P_{A0} \approx [uuv], u < v$) phase occurs only close to the ferroelectric R region. During the phase transformation from the T-side ferroelectric to the R-side ferroelectric (with temperature decrease or concentration of PT decrease), the polarization rotates along the $[100]_T$–$[uv0]_{Mc}$–$[uuv]_{Ma}$–$[111]_R$ path gradually, in a similar manner to the polarization rotation in $BiFeO_3$ near the MPB with varying strain field [31,45].

The exact structure in the MPB region has been under controversy for decades. Recently, an adaptive ferroelectric state theory was proposed by Jin and Wang [25,26], Wang [27,28], showing that the average M symmetry could be regarded as a result of coherence effects amongst R (or T) nanotwins. Two strain variants of the R phase (or T phase) can be adaptively considered to have monoclinic symmetry on average. (110) T nanotwins can be considered as Mc (or orthorhombic [21], which is a special case of Mc) on average [21,25,26,28,53], whereas (001) R nanotwins or (110) R nanotwins can mimic Ma and Mb on average [27,29], respectively. This theory involves the single phase with various local structures. Our model, on the contrary, supports the phase coexistence assumption. The adaptive ferroelectric state in the present study is a mixed phase state, not only mixed strain state. We show that R nanotwins and T nanotwins coexisting together locally can have M symmetry on average. There are two situations for phase coexistence between R twins and T twins: (1) (101) R twin + (101) T twin, which has been shown in our previous paper [51]; (2) (101) T twins + (001) R twins, which is the case in the present study. Furthermore, the present model can predict how the polarization rotates across the MPB region with changing

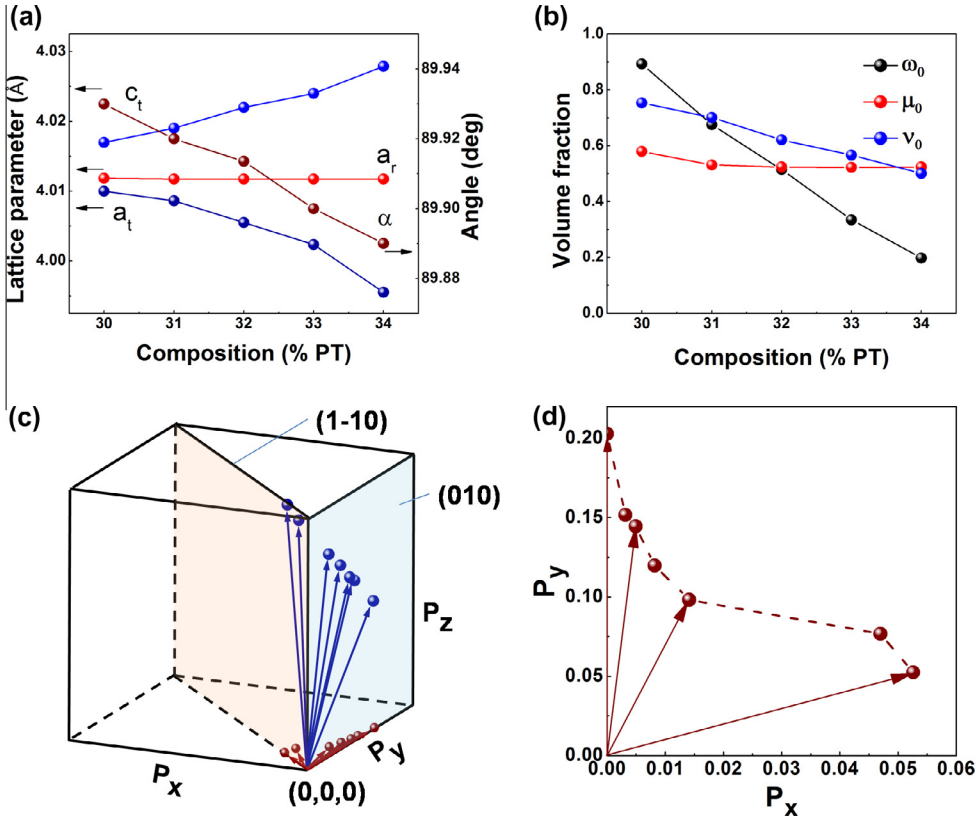

Fig. 6. (a) The lattice parameter vs. composition curves. The lattice parameters of R and T can be calculated from in situ XRD measurements by fitting the profiles with R and T symmetry using the Lorentz function. (b) The volume fractions μ_0, υ_0 and ω_0 as a function of composition. (c) The adaptive polarization vector in the MPB region as a function of composition. (d) The X–Y projection of the adaptive polarization vector.

temperature and composition, based on microstructural features (coexistence of R and T nanotwins).

5. Conclusions

We have proposed a phenomenological model to capture the gradual rotation of polarization as a function of temperature and composition in PMN–PT ceramics. Our TEM observations indicate that the local structure near the MPB region consists of the nanoscale coexistence of R and T twins, probably as a means to alleviate the transformation strain. Loading an external electric field or mechanical stress will result in a redistribution of the nanodomain variants, thus the nanodomain-averaged polarization will rotate with a gradual change of the nanodomain volume fractions μ, υ and ω. As a result, high electromechanical properties should be possible at the MPB.

Acknowledgements

The authors gratefully acknowledge the support of National Basic Research Program of China (Grant Nos. 2012CB619401 and 2010CB631003), National Natural Science Foundation of China (Grant Nos. 51302209, 51201126, 51321003, 51171140 and 51231008), and 111 project of China (B06025).

References

[1] Jaffe Jr WRC B, Jaffe H. Piezoelectric ceramics. New York: Academic Press; 1971.
[2] Seo Y-H, Vögler M, Isaia D, Aulbach E, Rödel J, Webber KG. Acta Mater 2013;61:6418.
[3] Hoffmann MJ, Hammer M, Endriss A, Lupascu DC. Acta Mater 2001;49:1301.
[4] Noheda B, Cox DE, Shirane G, Gao J, Ye ZG. Phys Rev B 2002;66.
[5] Lee HJ, Zhang S, Luo J, Li F, Shrout TR. Adv Funct Mater 2010;20:3154.
[6] Kholkin A, Morozovska A, Kiselev D, Bdikin I, Rodriguez B, Wu P, et al. Adv Funct Mater 2011;21:1977.
[7] Li F, Zhang S, Xu Z, Wei X, Shrout TR. Adv Funct Mater 2011;21:2118.
[8] Noheda B, Cox DE, Shirane G, Park SE, Cross LE, Zhong Z. Phys Rev Lett 2001;86:3891.
[9] Safari A, Akdoğan EK. Piezoelectric and acoustic materials for transducer applications. Berlin: Springer; 2008.
[10] Ma C, Guo H, Beckman SP, Tan X. Phys Rev Lett 2012;109:107602.
[11] Bhattacharya K, Ravichandran G. Acta Mater 2003;51:5941.
[12] Liu W, Ren X. Phys Rev Lett 2009;103:257602.
[13] Ahart M, Somayazulu M, Cohen RE, Ganesh P, Dera P, Mao H-K, et al. Nature 2008;451:545.
[14] Glazer AM, Thomas PA, Baba-Kishi KZ, Pang GKH, Tai CW. Phys Rev B 2004;70:184123.
[15] Gao J, Xue D, Wang Y, Wang D, Zhang L, Wu H, et al. Appl Phys Lett 2011;99:092901.
[16] Noheda B, Cox DE, Shirane G, Guo R, Jones B, Cross LE. Phys Rev B 2000;63:014103.
[17] Guo R, Cross LE, Park SE, Noheda B, Cox DE, Shirane G. Phys Rev Lett 2000;84:5423.

[18] Cox DE, Noheda B, Shirane G, Uesu Y, Fujishiro K, Yamada Y. Appl Phys Lett 2001;79:400.
[19] Dai X, Xu Z, Viehland D. Philos Mag B 1994;70:33.
[20] Viehland D, Kim M-C, Xu Z, Li J-F. Appl Phys Lett 1995;67:2471.
[21] Wang H, Zhu J, Zhang XW, Tang YX, Luo HS. Appl Phys Lett 2008;92:132906.
[22] Chang WS, Lim LC, Yang P, Miao H, Tu C-S, Chen Q, et al. Appl Phys Lett 2009;94:202907.
[23] Schönau KA, Knapp M, Kungl H, Hoffmann MJ, Fuess H. Phys Rev B 2007;76:144112.
[24] Schönau KA, Schmitt LA, Knapp M, Fuess H, Eichel R-A, Kungl H, et al. Phys Rev B 2007;75:184117.
[25] Jin YM, Wang YU, Khachaturyan AG, Li JF, Viehland D. J Appl Phys 2003;94:3629.
[26] Jin YM, Wang YU, Khachaturyan AG, Li JF, Viehland D. Phys Rev Lett 2003;91.
[27] Wang YU. Phys Rev B 2007;76:024108.
[28] Wang YU. Phys Rev B 2006;74:104109.
[29] Wang H, Zhu J, Zhang XW, Tang YX, Luo HS. J Am Ceram Soc 2008;91:2382.
[30] Vanderbilt D, Cohen MH. Phys Rev B 2001;63:094108.
[31] Chen Z, Luo Z, Huang C, Qi Y, Yang P, You L, et al. Adv Funct Mater 2011;21:133.
[32] Bai F, Li J, Viehland D. Appl Phys Lett 2004;85:2313.
[33] Bai F, Li J, Viehland D. J Appl Phys 2005;97:054103.
[34] Kutnjak Z, Petzelt J, Blinc R. Nature 2006;441:956.
[35] Ohwada K, Hirota K, Rehrig PW, Fujii Y, Shirane G. Phys Rev B 2003;67:094111.
[36] Davis M, Damjanovic D, Setter N. Phys Rev B 2006;73:014115.
[37] Kiat J-M, Uesu Y, Dkhil B, Matsuda M, Malibert C, Calvarin G. Phys Rev B 2002;65:064106.
[38] Singh AK, Pandey D. Phys Rev B 2003;67:064102.
[39] Fu H, Cohen RE. Nature 2000;403:281.
[40] Jang HW, Baek SH, Ortiz D, Folkman CM, Das RR, Chu YH, et al. Phys Rev Lett 2008;101:107602.
[41] Ouyang J, Roytburd AL. Acta Mater 2006;54:5565.
[42] Ouyang J, Zhang W, Huang X, Roytburd AL. Acta Mater 2011;59:3779.
[43] Zhang JX, Xiang B, He Q, Seidel J, Zeches RJ, Yu P, et al. Nat Nano 2011;6:98.
[44] Zeches RJ, Rossell MD, Zhang JX, Hatt AJ, He Q, Yang C-H, et al. Science 2009;326:977.
[45] Christen HM, Nam JH, Kim HS, Hatt AJ, Spaldin NA. Phys Rev B 2011;83:144107.
[46] George A, Rossetti J, Khachaturyan AG. Appl Phys Lett 2007;91:072909.
[47] Heitmann AA, Rossetti GA. Philos Mag 2009;90:71.
[48] George A, Rossetti J, Zhang W, Khachaturyan AG. Appl Phys Lett 2006;88:072912.
[49] Rossetti GA, Khachaturyan AG, Akcay G, Ni Y. J Appl Phys 2008;103:114113.
[50] Bhattacharya K. Microstructure of martensite: why it forms and how it gives rise to the shape-memory effect. New York: Oxford University Press; 2003.
[51] Wu H, Xue D, Lv D, Gao J, Guo S, Zhou Y, et al. J Appl Phys 2012;112:052004.
[52] Ye ZG, Noheda B, Dong M, Cox D, Shirane G. Phys Rev B 2001;64:184114.
[53] Wang H, Zhu J, Lu N, Bokov AA, Ye Z-G, Zhang XW. Appl Phys Lett 2006;89:042908.
[54] Schierholz R, Fuess H. Phys Rev B 2011;84:064122.
[55] Kim K-H, Payne DA, Zuo J-M. Phys Rev B 2012;86:184113.
[56] Shang JK, Tan X. Acta Mater 2001;49:2993.
[57] Cai Y, Phillipp F, Zimmermann A, Zhou L, Aldinger F, Rühle M. Acta Mater 2003;51:6429.
[58] Van Aert S, Turner S, Delville R, Schryvers D, Van Tendeloo G, Salje EKH. Adv Mater 2012;24:523.
[59] Cheng SY, Ho NJ, Lu HY. J Am Ceram Soc 2006;89:2177.
[60] Khachaturyan A, Shapiro S, Semenovskaya S. Phys Rev B 1991;43:10832.
[61] Lieberman DS, Wechsler MS, Read TA. J Appl Phys 1955;26:473.
[62] Wechsler M, Lieberman D, Read T. Am Inst Min(Metall) Eng 1953;197:1503.